<Original Article>

Renoprotective Effects of Chymase Inhibition on Cisplatin-Induced Nephrotoxicity in Mice

Masanari YOSHIMOTO[1,2], Denan JIN[1], Hiroshi SAKONJO[2], and Shinji TAKAI[1]

1 Department of Innovative Medicine, Graduate School of Medicine, Osaka Medical and Pharmaceutical University, Takatsuki, Osaka 569-8686, Japan

2 Research Department, NISSEI BILIS Co. Ltd., Minakuchi, Koka, Shiga 528-0052, Japan

Key words: cisplatin, nephrotoxicity, chymase, chymase inhibitor

ABSTRACT

Although cisplatin is a useful antitumor drug, its nephrotoxicity is a critical limiting factor for this chemotherapy. The present study examined if mast cell-derived chymase might contribute to this pathology, through analysis of the pattern of chymase expression, as well as the effects of chymase inhibition, in a mouse cisplatin-induced nephrotoxicity model. We found that mast cells positive for the chymase, murine mast cell protease-4 (MMCP-4), and MMCP-4 mRNA expression in kidney tissues increased largely during the acute phase after cisplatin injection. Increase in serum creatinine and blood urea nitrogen, as well as histopathological changes such as renal tubular enlargement, were also observed in cisplatin-injected mice. Only half of the cisplatin-injected mice survived during the 6-day observation period. mRNA expression of reactive oxygen species-related factors, as well as inflammation-related factors, such as NOX2 and TNF-α, were all significantly increased in the acute phase after cisplatin injection. On the other hand, reduction in mast cell-derived chymase expression, along with improvement in renal function, histopathological changes, and survival rates, were observed in cisplatin-induced nephrotoxic mice treated with a chymase-specific inhibitor, suggesting that chymase plays an important role in cisplatin-induced nephrotoxicity in mice.

INTRODUCTION

Cisplatin is a platinum-based chemotherapeutic drug that is wildly used to treat solid cancers, such as head, neck, cervical, ovarian, testicular, and other types of malignant tumors [1, 2]. However, the side effect of nephrotoxicity during use of cisplatin is a critical limiting factor in the use of this cancer chemotherapy [3]. Cisplatin is a non-cell cycle-specific antitumor agent, and its chemotherapeutic mechanisms are attributed to the covalent binding of platinum to the purine bases guanine and adenine in rapidly dividing cells. This covalent binding reportedly leads to intra-strand and inter-strand DNA crosslinks, causing subsequent strand breakage and damage. During subsequent DNA repair processes, these cells often undergo apoptotic or non-apoptotic cell death due to remnant damaged DNA, RNA, and proteins [4–6]. Unfortunately, the cytotoxic effects of cisplatin are usually not limited to malignant tumor cells, and also affect normal tissues in multiple organs, such as the kidney, bone marrow, and

Address correspondence to:
Denan Jim, Department of Innovative Medicine, Graduate School of Medicine, Osaka Medical and Pharmaceutical University, 2–7 Daigaku-machi, Takatsuki, Osaka 569–8686, Japan.
Phone: +81−72−683−1221 Fax: +81−72−684−6730 Email: denan.jin@ompu.ac.jp

nerves. Among them, nephrotoxicity is the most commonly encountered problem in clinical practice. Cisplatin accumulates selectively in the proximal tubule through basolateral-to-apical transport, disrupting mitochondrial energetics and endoplasmic reticulum Ca^{2+} homeostasis by stimulating reactive oxygen species (ROS) and pro-inflammatory cytokine production [7–9]. Reportedly, approximately 25–40 % of cancer patients treated with cisplatin exhibit a progressive decline in renal function [7], limiting continuation of medical treatment by cisplatin in these patients. Although, of course, various measures have been taken to overcome the kidney injury, such as hydration regimens, almost 4–23 % of patients still develop nephrotoxicity, and are unable to continue treatment [10]. Therefore, it is necessary to find methods to deal with this side effect as soon as possible.

Recently, mast cell-derived chymase, as a new member of the renin angiotensin system (RAS), has begun to attract a lot of attention [11]. Following its degranulation under certain circumstances, such as ischemic or inflammatory conditions, chymase, as angiotensin converting enzyme (ACE), able to cleave angiotensin (Ang) I to Ang II. In addition to Ang II-generating properties, chymase can also activate pro-matrix metalloproteinases (MMP)-9 and latent transforming growth factor (TGF)-β1 to their active forms [12, 13]. As is well known, Ang II promotes superoxide production through activation of NADPH oxidase (NOX) [14], and these products release several inflammation-related cytokines, such as tumor necrosis factor (TNF)-α, interleukin (IL)-1β, and IL-6, by the activation of nuclear factor-kappa B (NF-κB) [15, 16]. Interestingly, MMP-9 and TGF-1β are also known to be important mediators in organ fibrotic disorders after inflammatory events [17]. Since chymase is involved in the activation of not only Ang II, but also MMP-9 and TGF-β1, and in view of the fact that ROS and inflammatory events are critical mediators in the development of cisplatin-induced nephrotoxicity, we evaluated the relationship between mast cell-derived chymase and cisplatin-induced nephrotoxicity through analysis of the pattern of chymase expression, as well as the effects of chymase inhibition in the present study.

METHODS

Animals and materials

Six-week-old male BALB/c mice weighing 18–20 g were purchased from Japan SLC (Shizuoka, Japan), and were maintained under 12-h light/12-h dark conditions. Temperature and humidity were controlled, and the animals had free access to water and standard laboratory diet. All animal procedures were approved by the Committee of Animal Use and Care of Osaka Medical and Pharmaceutical University (Approval code number; AM234-024) and performed in accordance with the Guidelines for Animal Research. TY-51469 was synthesized as a specific chymase inhibitor and obtained from Toaeiyo Ltd. (Tokyo, Japan) [18].

Experimental design

A single 20 mg/kg dose of cisplatin was administered intraperitoneally to reproduce the clinical nephrotoxicity of cisplatin. The animals were divided into the following experimental groups:

• Group 1 (Normal): Six-week-old male BALB/c mice (n = 6) without administration of cisplatin served as the control group for all cisplatin-treated groups.

• Group 2 (Placebo): Six-week-old male BALB/c cisplatin-treated mice (n = 12) served as the placebo group. Half of these animals were sacrificed on day 1 and the remaining half were sacrificed on day 3.

• Group 3 (TY-51469-treated group): Six-week-old male BALB/c mice (n = 12) treated with 30 mg/kg/day of the chymase-specific inhibitor (TY-51469), initiated 1 hour before injection of cisplatin, served as the TY-51469-treated group. Half each of these animals were sacrificed on day 1 and day 3, respectively.

• Group 4 (placebo): Six-week-old male BALB/c mice (n = 20) treated with cisplatin served as the placebo group for the survival experiment.

• Group 5 (TY-51469-treated group): Six-week-old male BALB/c mice (n = 20) treated with 30 mg/kg/day of TY-51469, initiated 1 hour before injection of cisplatin, served as the TY-51469-treated group in the survival experiment. Survival rates in Groups 4 and 5 were evaluated on day 6 after the cisplatin injection.

Sample processing

At the endpoints in each group, the left kidneys of the mice were removed after whole blood sample collection under pentobarbital anesthesia. The next day, the collected blood samples were centrifuged at 3,000 rpm for 15 min and serum was separated. Serum creatinine (Scr) and blood urea nitrogen (BUN) were measured by SRL Inc. (Tokyo, Japan). The resected left kidneys were washed in ice cold saline, one half of each kidney was immediately stored at −80 °C for real-time polymerase chain reaction (RT-PCR) examination, and the other half was immediately fixed in Carnoy's fixative overnight. The fixed renal tissues were embedded in paraffin for later histological examinations.

Histological analysis

For histological and immunohistological stainings, 3-μm-thick serial cross-sections were prepared from paraffin blocks of the kidneys by using a sliding microtome (Litoratomu, REM-710, Yamato Koki Kogyo Ltd., Saitama, Japan). The sections were mounted on adhesive glass slides (Matsunami Glass Ind., Kishiwada, Japan), and histological changes in the kidney were assessed using standard Peri-

odic acid–Schiff (PAS) staining. Toluidine blue staining was also performed to identify mast cell distribution. Briefly, after deparaffinization with lemosol (Wako Pure Chemicals, Osaka, Japan), the sections were immersed in 0.5 % toluidine blue solution (pH 4.8) for around 15 min, fractionated with 0.5 % glacial acetic acid solution, and mounted after drying.

To identify chymase distribution, immunohistological examinations were also performed on the serial cross-sections adjacent to those used for mast cell staining by using an anti-murine mast cell protease-4 (anti-MMCP-4 antibody) (ab92368, Abcam, Cambridge, UK), according to a protocol described elsewhere [19]. Briefly, to suppress endogenous peroxidase activity and nonspecific binding, the deparaffinized sections were incubated with 3 % hydrogen peroxide and protein-blocking solution, respectively, for 5 min at room temperature. Then, the sections were incubated overnight at 4 °C with the above diluted primary antibodies (1:100), followed by reaction with components from a labeled streptavidin-biotin peroxidase kit (Dako LSAB kit, Carpinteria, CA, USA) that included 3-amino-9-ethylcarbazole color development. The sections were then lightly counterstained with hematoxylin, and finally, mounted with cover glasses. Following the above staining procedures, the number of mast cells and chymase-positive cells in the sections from experimental groups were evaluated under a computerized morphometry system (NIS-Elements Documentation, version (v) 3.07, Nikon, Tokyo, Japan) and the number of cells per unit area were compared between each group.

Real-time polymerase chain reaction (RT-PCR)

Renal total RNA was extracted using Trizol reagent (Life Technologies, Rockville, MD, USA) and subsequently dissolved in RNase-free water (Takara Bio Inc., Otsu, Japan) [20]. Total RNA (1 μg) was transcribed into cDNA with Superscript VIRO (Invitrogen, Carlsbad, CA, USA). Then, mRNA levels were measured by RT-PCR on a Stratagene Mx3000P RT-PCR system (Agilent Technologies, San Francisco, CA, USA) using TaqMan fluorogenic probes. RT-PCR primers and probes for MMCP-4, NADPH oxidase (NOX)2, TGF-β1, MMP-9, IL-1β, IL-6, TNF-α, and 18S ribosomal RNA (rRNA) were designed by Roche Diagnostics (Tokyo, Japan).

The primers used were as follows: 5’-ggcctgtaaaaactattg gcatt-3’ (forward) and 5-cacacagtagaggtcctccaga-3’ (reverse) for MMCP-4, 5’-tgccaacttcctcagctaca-3’(forward) and 5’-gtg cacagcaaagtgattgg-3’ (reverse) for NOX2, 5’-ctgaatcctcgatg gaatgg-3’ (forward) and 5’-ccatggcccctacaatctt-3’ (reverse) for myeloperoxidase (MPO), 5’-tggagcaacatgtggaactc-3’ (forward) and 5’-cagcagccggttaccaag-3’ (reverse) for TGF-β1, 5’-gaatgccccattctgcac-3’ (forward) and 5’-gggtttagtttctgc aaactgc-3’ (reverse) for MMP-9, 5’-agttgacggaccccaaaag-3’ (forward) and 5’-agctggatgctctcatcagg-3’ (reverse) for IL-1β, 5’-gctaccaaactggatataatcagga-3’ (forward) and 5’-ccaggtagct atggtactccagaa-3’ (reverse) for IL-6, 5’-aggcgaagattactgccaa g-3’ (forward) and 5’-catggctatgaggtagagacagg-3’ (reverse) for TNF-α, and 5’-gcaattattccccatgaacg-3’ (forward) and 5’ -gggacttaatcaacgcaagc-3’ (reverse) for 18S rRNA.

The following probes were used: 5’-tccaggtc-3’ for MMCP-4, 5’-ctggctgg-3’ for NOX2, 5’-ccaggagg-3’ for MPO, 5’-ttcctggc-3’ for TGF-β, 5’-ctccttcc-3’ for MMP-9, 5’-ctgc ttcc-3’ for IL-1β, 5’-ttcctctg-3’ for IL-6, 5’-agccccag-3’ for TNF-α, and 5’-ttcccagt-3’ for 18S rRNA. The mRNA levels of the above factors were normalized to those of 18S rRNA.

Statistical analysis

All numerical data are expressed as means ± standard error of the mean (SEM). Significant differences among the mean values of multiple groups were evaluated by one-way analysis of variance (ANOVA) followed by post hoc analysis (Fisher’s test). Survival data are presented as Kaplan-Meier curves. The survival curves of individual groups were compared using the log-rank test. $P < 0.05$ was considered significant.

RESULTS

Compared with the normal group, body weight (BW) in the placebo group decreased largely 3 days after cisplatin injection. Chymase-specific inhibitor TY-51469 treatment did not decrease the loss of weight (**Figure 1**). A single injection of cisplatin in the placebo group resulted in a significant increase in serum Scr and BUN levels on day 3 of observation. On the other hand, these elevations were largely suppressed with the continued TY-51469 treatment (**Figure 1**).

Survival rates in the placebo group decreased to about 50 % at 6 days after cisplatin treatment, while the survival rate in the TY-51469-treated group was about 80 % ($p < 0.05$, **Figure 2**).

Figure 3 shows representative images of PAS staining in sections from mice in the normal, placebo and TY-51469-treated groups. As can be seen in the photo of PAS staining in the normal group, there was no noticeable enlargement of the renal tubules and glomeruli (yellow arrows). However, although not seen in all the mice, enlargement of the renal tubules (black asterisks) was observed in some cisplatin-injected placebo mice. These pathological changes were ameliorated to some extent in the TY-51469-treated group.

Figure 4 presents typical images of PAS staining in the placebo and TY-51469 groups showing pathological changes in kidney tissues over time. In the placebo group, pathological changes in renal tissue, such as enlargement of the renal tubules, was detectable 3 days after cisplatin treatment, with the changes becoming very noticeable on day 6. Such time-dependent pathological changes were ameliorated in the TY-51469-treatment group. Regrettably, it was

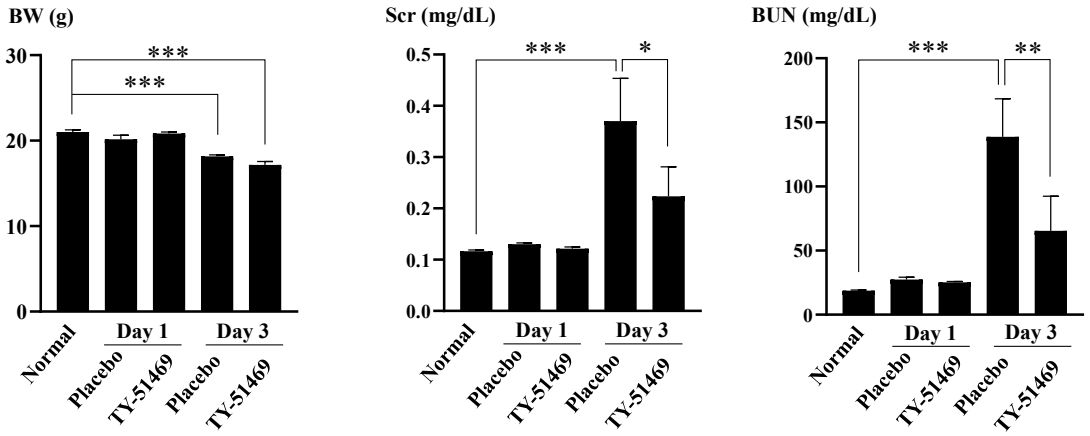

Figure 1 **Changes in body weight, Scr, and BUN levels in normal, placebo, and TY-51469-treated groups. *$P < 0.05$, **$P < 0.01$, ***$P < 0.001$.**

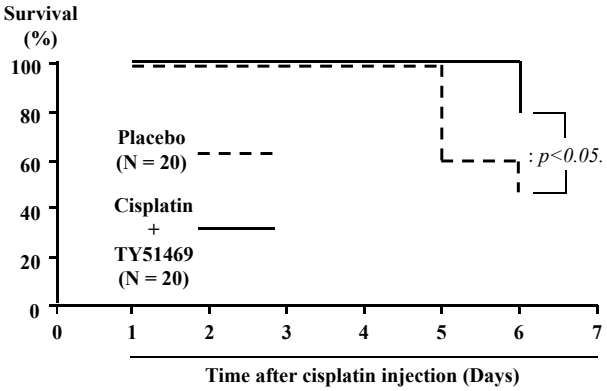

Figure 2 **Cumulative survival rates 6 days after injection of cisplatin in mice treated with placebo (n = 20) or the chymase inhibitor TY-51469 (n = 20).**

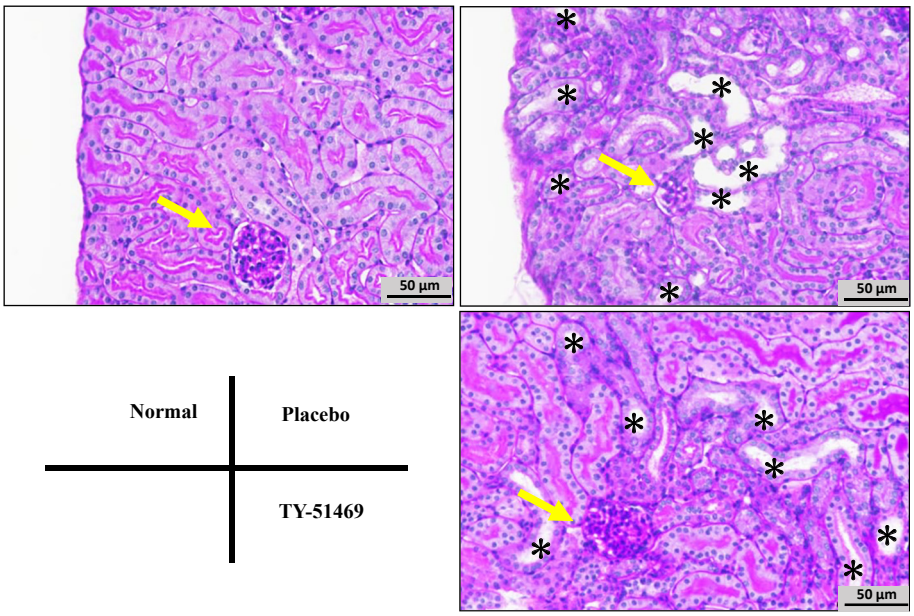

Figure 3 **Representative PAS stained images from normal, placebo, and TY-51469-treated groups.** The yellow arrows indicate the glomerulus and black asterisks indicate enlarged renal tubules.

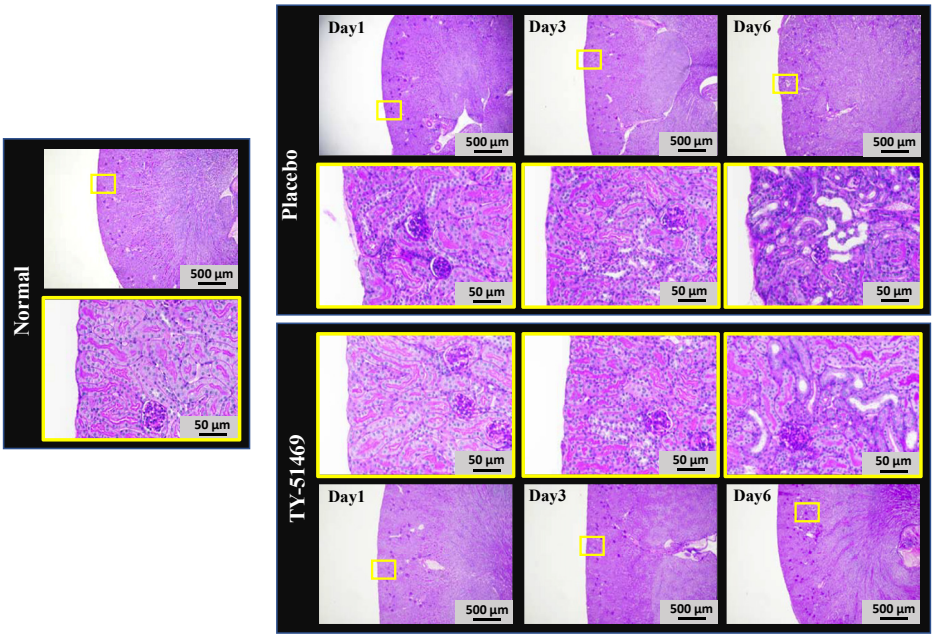

Figure 4 **Typical PAS-stained images showing pathological changes in kidney tissues from cisplatin-treated mice, as well as in mice treated with TY-51469, at 1, 3, and 6 days after cisplatin injection.**

not feasible in this study to quantify the extent of kidney tissue injury, such as enlargement of the renal tubules caused by cisplatin, due to significant individual variations.

Figure 5 shows representative toluidine blue staining and MMCP-4 immunostaining in serial sections from the kidneys of normal and 1 day after cisplatin-injected mice, respectively. Staining of mast cells and MMCP-4-positive cells using adjacent serial sections allow identification of not only MMCP-4 storage cells, but also enable differentiation of different types of mast cells. Since the diameter of mast cells is about 20 μm, when the cross-sections are about 4 μm in thickness, the rate of appearance of the same mast cell in two serial cross-sections is comparatively high. As can be seen in the normal kidney section in **Figure 5**, toluidine blue staining detected the presence of two mast cells in the cortical region of the kidney (red arrows), although no MMCP-4-positive staining was visible in the locus where mast cells should have been in the adjacent serial section (green arrows), indicating that these mast cells only expressed tryptase, and were of the MC_T-type.

On the other hand, in placebo kidneys 1 day after cisplatin injection, toluidine blue staining also detected the presence of two mast cells in the cortical region of the kidney (red arrows), while MMCP-4 immunostaining performed on the serial section adjacent to toluidine blue staining confirmed one of them to be positive for MMCP-4 (red arrows). indicating that this mast cell expressed both tryptase and chymase and belonged to the MC_{TC}-type.

Figure 6 shows changes in the number of mast cells and MMCP-4-positive cells, as well as the expression level of MMCP-4 mRNA in each group at 1 and 3 days after cisplatin injection. As can be seen in the bar graphs of **Figure 6**, the number of renal mast cells in the placebo group at 1 and 3 days after cisplatin injection were unchanged as compared to the normal group. On the other hand, we did not find a significant difference in the number of mast cells between the cisplatin-injected placebo group and the TY-51469-treated group on either day 1 or day 3 of the observation period. Interestingly, compared with the normal group, MMCP-4-positive cells were significantly increased in the placebo group on day 1 after cisplatin injection. On the other hand, MMCP-4-positive cells in the kidney were reduced significantly with TY-51469 treatment on day 1 after cisplatin injection. Although MMCP-4-positive cells in the placebo group were largely decreased on day 3 rather than day 1 after cisplatin injection, their numbers still remained high as compared to the normal group.

The number of MMCP-4-positive cells tended to decrease on day 3 after TY-51469 treatment as compared to the placebo group. Compared to the normal group, mRNA expression of MMCP-4 tended to increase on both day 1 and day 3 after cisplatin injection in the placebo group. On the other hand, mRNA expression by MMCP-4 was significantly suppressed by treatment with TY-51469.

In the present study, we also evaluated the expression profiles of some inflammation-related cytokines, such as IL-1β, IL-6, and TNF-α after injection of cisplatin. As can be seen in **Figure 7**, the expression level of IL-1β mRNA increased significantly in the placebo group on day 1 after cisplatin injection, and this elevation was significantly suppressed with TY-51469 treatment. A similar pattern was also observed for IL-6 mRNA expression. Compared with

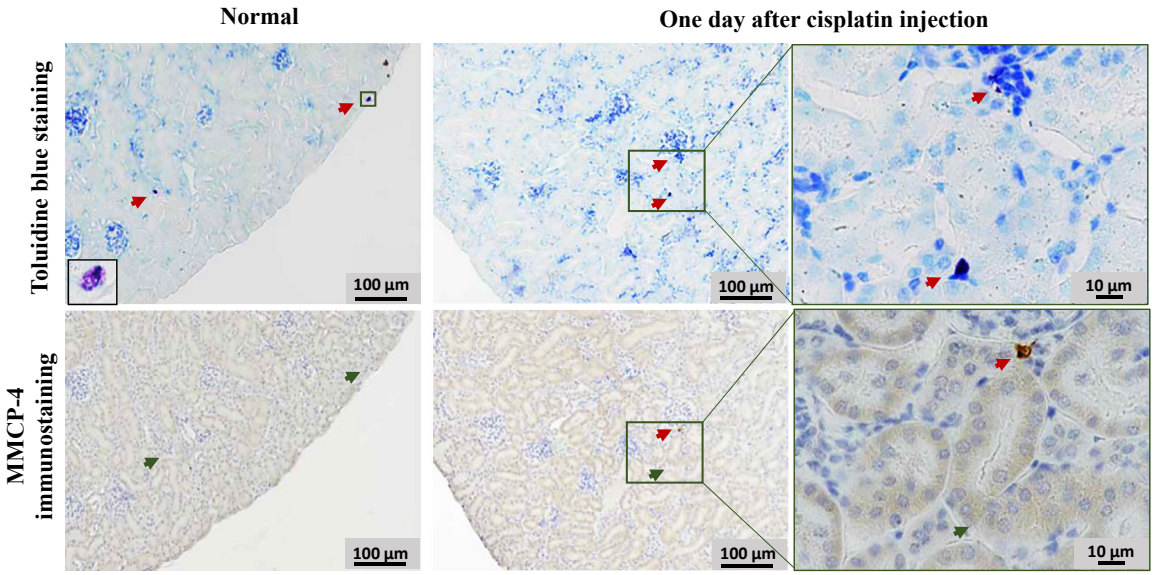

Figure 5 **Representative toluidine blue staining and MMCP-4 immunostaining in serial kidney sections from normal mice and those 1 day after cisplatin injected placebo group.**
The red arrows in the upper photos showing toluidine blue staining indicate areas of localization of mast cells. The lower panel shows immunostaining for MMCP-4 on serial sections obtained adjacent to the above toluidine blue stained sections. As can be seen in these photos, some mast cells did not express MMCP-4 in the areas where the mast cells should have been (green arrows), while some mast cells did express MMCP4 (red arrows).

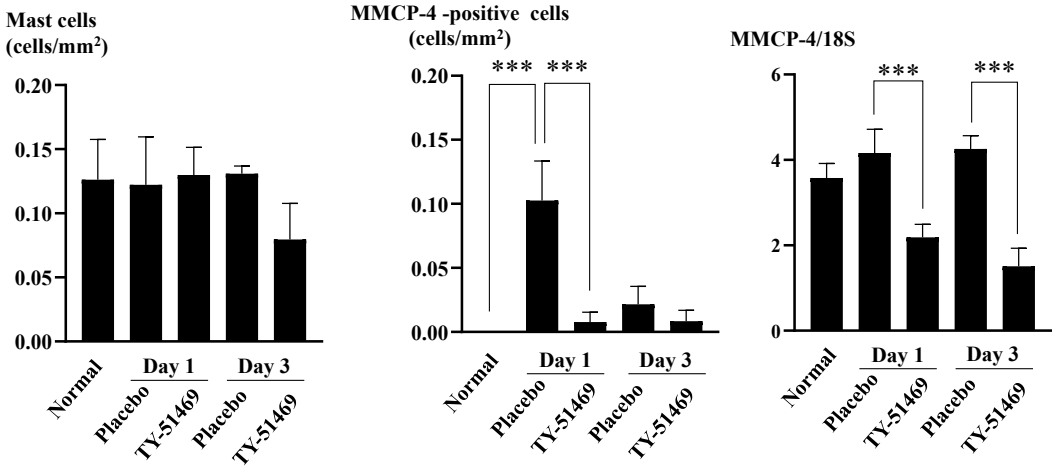

Figure 6 **Quantitative analysis of mast cells and MMCP-4-positive cells, as well as MMCP-4 mRNA expression levels in kidney tissues from normal, placebo, and TY-51469-treated groups.**
***$P < 0.001$.

the normal group, mRNA expression of TNF-α in the placebo group tended to increase from day 1, and significantly increased on day 3 of the observation period after cisplatin injection. On the other hand, TY-51469 treatment suppressed these elevations to some extent on both day 1 and day 3 (**Figure 7**).

Figure 8 shows the mRNA expression of some ROS-related factors, such as NOX2 and MPO, as well as fibrosis-related factors, such as TGF β1 and MMP-9, after cisplatin injection. As can be seen in the upper panel of **Figure 8**, compared to the normal group, expression levels of NOX2 mRNA were increased at all the observation points after cisplatin injection in the placebo group.

Further, TY-51469 treatment significantly suppressed these elevations. The expression level of MPO mRNA in the placebo group tended to increase from day 1, and significantly increased at 3 days after cisplatin injection. On the other hand, TY-51469 treatment suppressed these ele-

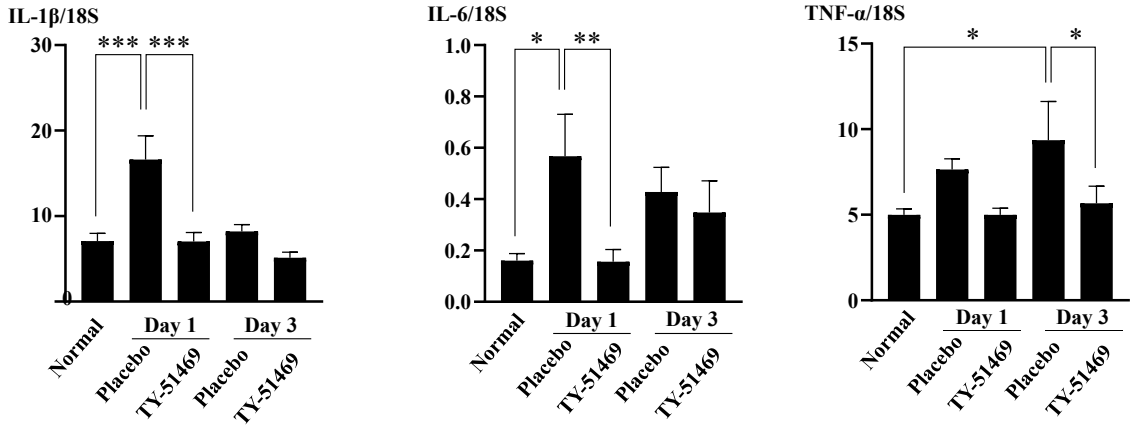

Figure 7 **Changes in IL-1β, IL-6, and TNF-α mRNA expression levels in kidney tissues from normal, placebo, and TY-51469-treated groups.**
*$P < 0.05$, **$P < 0.01$, ***$P < 0.001$.

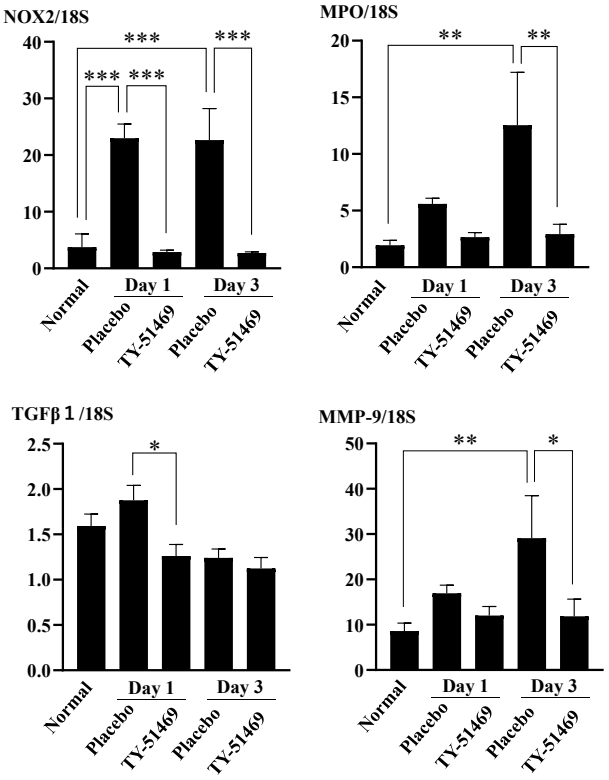

Figure 8 **Changes in NOX2, MPO, TGF β1, and MMP-9 mRNA expression levels in kidney tissues from normal mice and mice treated with placebo or TY-51469.**
*$P < 0.05$, **$P < 0.01$, ***$P < 0.001$.

vations to some extent. The expression level of TGF β1 mRNA in the placebo group also tended to increase 1 day after cisplatin injection, and it was significantly suppressed with TY-51469 treatment. The expression level of MMP-9 mRNA in the placebo group also tended to increase from day 1, with a significant increase on day 3 after cisplatin injection. TY-51469 treatment suppressed these elevations to some extent (**Figure 8**).

DISCUSSION

Unlike humans, mice express several types of chymases, such as murine mast cell protease 1 (MMCP-1), MMCP-2 MMCP-3, MMCP-4, etc., with variable enzymatic properties [21]. Among them, MMCP-4 has been reported to be most similar to human chymase in terms of Ang II generation [22, 23]. In the present study, we focused on chymase to examine if MMCP-4 might participate in the cisplatin-induced nephrotoxic pathology in mice. We found that the kidneys of normal mice primarily expressed MC_T-type mast cells that do not contain chymase. However, in cisplatin-treated mice, while the overall number of mast cells, as determined by toluidine blue staining, remained largely unchanged, there was a noticeable shift in the ratio of MC_T-type to MC_{TC}-type mast cells. As depicted in the bar graph in **Figure 6**, the MMCP-4-positive mast cells and MMCP-4 gene expression were all largely increased during the acute phase after cisplatin injection, with suppression of these expressions by treatment with the chymase-specific inhibitor, TY-51469, with beneficial effects on renal pathological changes and function, as well as survival rates. These findings suggest that activation of renal mast cell-derived chymase after cisplatin administration might be harmful, and that chymase inhibition might enable mitigation of cisplatin-induced side effects.

Cisplatin is a chemotherapeutic drug that has been widely used for the treatment of various cancers. However, its use is limited by the side effect of severe nephrotoxicity. Cisplatin-induced nephrotoxicity is characterized by renal tubular cell necrosis, tissue damage, renal dysfunction, and acute kidney failure [9]. The injurious effects of cisplatin are likely caused by ROS and inflammatory processes in

the kidney. For example, the role of an interaction between cisplatin and DNA in the generation of superoxide radicals has been documented in in vitro assays [24]. In addition, the results of both in vitro and in vivo experiments have indicated that reducing ROS production by oxygen radical scavengers might protect against cisplatin-mediated cytotoxicity, further substantiating the direct role of ROS [25]. On the other hand, inflammatory events could further amplify the ROS-mediated direct nephrotoxicity of cisplatin. For example, in previous studies, renal expression of TNF-α was increased significantly after cisplatin injection in mice [26], and TNF-α inhibition or knockout reduced cisplatin-induced renal dysfunction, histologic renal injury and mortality rate [27]. In the present study, we found that the mRNA expression of ROS-related factors, such as NOX2, the subunit of NADPH oxidase and MPO, as well as inflammation-related factors, such as TNF-α, IL-1β, and IL-6, were all increased significantly during the acute phase after cisplatin injection. These expressions were also largely suppressed by treatment with the chymase-specific inhibitor, TY-51469. This suggests that the antioxidant and anti-inflammatory effects of chymase inhibition in this study did indeed exert some beneficial effects on renal function and survival rate. Why do excessive production of ROS and inflammatory reactions have a negative impact on organs? First, ROS, such as superoxide anion (O_2^-) and hydrogen peroxide (H_2O_2), are highly reactive molecules that can damage cellular components, including lipids, proteins, and DNA (28). For example, ROS can impair endothelial function by reducing nitric oxide (NO) bioavailability, thereby promoting vasoconstriction, inflammation, and thrombosis (29). This endothelial dysfunction might contribute to renal vasoconstriction and decreased renal blood flow, thereby exacerbating kidney injury. Moreover, ROS serve as signaling molecules that activate inflammatory pathways, such as NF-κB, leading to the production of pro-inflammatory cytokines and chemokines [26]. As is well known, an excessive inflammatory response might also result in tissue damage and leukocyte infiltration in the kidney. Thus, chymase inhibitors appear to have a beneficial effect on reducing active oxygen production in this model. As can be seen in **Figure 1** and **2**, the levels of Scr and BUN in mouse blood increased significantly 3 days after cisplatin injection, and the survival rate in the placebo group was only approximately 50 %. On the other hand, TY-51469 treatment was associated with a reduction in blood levels of Cre and BUN, as well as increase in the survival rate to approximately 80 %. Moreover, pathological changes in kidney tissue, such as renal tubular enlargement due to necrosis, also improved following treatment with the chymase-specific inhibitor (**Figure 4**), indicating that activation of renal chymase in the present model was indeed harmful.

Based on the above experimental evidence, it seems clear that activation of chymase does indeed contribute to enhancement of nephrotoxicity after cisplatin administration. But how does chymase activation promote oxidative stress and inflammatory events in this model? We consider the overproduction of Ang II due to chymase activation during the acute phase after cisplatin injection to be partly responsible for the pathogenesis of cisplatin-induced nephrotoxicity in this model. It was previously reported that Ang II stimulates superoxide production through NOX activation [14], and that overproduction of the superoxide can activate NF-κB, which is the main signaling pathway in inflammatory events [15]. For example, release of certain inflammation-related cytokines, such as TNF-α, IL-1β, and IL-6, were all dramatically increased by NF-κB activation [30]. It was also reported in a rat cisplatin-injected model that treatment with the angiotensin receptor blocker, candesartan, is capable of improving renal and lung injury through its anti-inflammatory and antioxidant effects [31, 32]. Taken together, we can speculate that the increase in chymase activity after cisplatin injection leads to an increase in chymase-dependent Ang II production, which, in turn, enhances cisplatin-induced direct nephrotoxicity through the Ang II-ROS-NF-κB axis.

In the present study, we also found that fibrosis-related factors, such as TGF β1 and MMP-9, were also largely increased after the injection of cisplatin. Since, apart from its Ang II-forming property, chymase can also activate pro-MMP-9 and latent TGF-β1, our study also suggests an additional role of chymase in the pathogenesis of renal fibrosis during the late phase of cisplatin-induced nephrotoxicity, although chronic examinations were not performed in the present study.

In conclusion, along with the reduction of mast cell-derived chymase expression, treatment with a chymase-specific inhibitor significantly improved renal function and pathological changes, as well as survival rates in a cisplatin-induced mouse nephrotoxicity model, suggesting that cisplatin might exert its detrimental effects on kidney function via activation of chymase, and that chymase inhibition might be a target for mitigation of cisplatin-induced side effects.

AUTHOR CONTRIBUTIONS

Masanari Yoshimoto and Denan Jin conceived and managed the study and wrote the manuscript. Masanari Yoshimoto and Hiroshi Sakonjo constructed the mouse model of cisplatin-induced nephrotoxicity. Masanari Yoshimoto and Shinji Takai performed histological and gene expression examinations. All authors have read and agreed to the published version of the manuscript.

FUNDING

This study was supported in part by Grants-in-Aid

17K09741, 24590336, 21590295, 15590240, 13670102, and 20K08601 for Scientific Research (C) from the Ministry of Education, Science, Sports and Culture, Japan.

DISCLOSURE STATEMENT

The authors declare no conflicts of interest.

REFERENCES

1. Dasari S, Tchounwou PB. Cisplatin in cancer therapy: molecular mechanisms of action. *Eur J Pharmacol.* 2014;740:364–378. doi: 10.1016/j.ejphar.2014.07.025.
2. Ghosh S. Cisplatin: the first metal based anticancer drug. *Bioorg Chem.* 2019;88:102925. doi: 10.1016/j.bioorg.2019.102925.
3. Hoek J, Bloemendal KM, van der Velden LA, et al. Nephrotoxicity as a dose-limiting factor in a high-dose cisplatin-based chemoradiotherapy regimen for head and neck carcinomas. *Cancers.* 2016;8(2):21. doi: 10.3390/cancers8020021.
4. Riddell IA. Cisplatin and oxaliplatin: our current understanding of their actions. *Met Ions Life Sci.* 2018;18. doi: 10.1515/9783110470734-007.
5. Aggarwal SK. A histochemical approach to the mechanism of action of cisplatin and its analogues. *J Histochem Cytochem.* 1993;41(7):1053–1073. doi: 10.1177/41.7.8515048.
6. Chválová K, Brabec V, Kaspárková J. Mechanism of the formation of DNA-protein cross-links by antitumor cisplatin. *Nucleic Acids Res.* 2007;35(6):1812–1821. doi: 10.1093/nar/gkm032.
7. Miller RP, Tadagavadi RK, Ramesh G, Reeves WB. Mechanisms of cisplatin nephrotoxicity. *Toxins.* 2010;2(11):2490–2518. doi: 10.3390/toxins2112490.
8. Manohar S, Leung N. Cisplatin nephrotoxicity: a review of the literature. *J Nephrol.* 2018;31(1):15–25. doi: 10.1007/s40620-017-0392-z.
9. Ozkok A, Edelstein CL. Pathophysiology of cisplatin-induced acute kidney injury. *Biomed Res Int.* 2014;2014:967826. doi: 10.1155/2014/967826.
10. Mi XJ, Hou JG, Wang Z, et al. The protective effects of maltol on cisplatininduced nephrotoxicity through the AMPK-mediated PI3K/Akt and p53 signaling pathways. *Sci Rep.* 2018;8(1):15922. doi: 10.1038/s41598-018-34156-6.
11. Takai S, Shiota N, Yamamoto D, Okunishi H, Miyazaki M. Purification and characterization of angiotensin II-generating chymase from hamster cheek pouch. *Life Sci.* 1996;58(7):591–597. doi: 10.1016/0024-3205(95)02328-3.
12. Lindstedt KA, Wang Y, Shiota N, et al. Activation of paracrine TGF-beta1 signaling upon stimulation and degranulation of rat serosal mast cells: a novel function for chymase. *FASEB J.* 2001;15(8):1377–1388. doi: 10.1096/fj.00-0273com.
13. Fang KC, Raymond WW, Lazarus SC, Caughey GH. Dog mastocytoma cells secrete a 92-kD gelatinase activated extracellularly by mast cell chymase. *J Clin Investig.* 1996;97(1):1589–1596. doi: 10.1172/JCI118583.
14. Griendling KK, Minieri CA, Ollerenshaw JD, Alexander RW. Angiotensin II stimulates NADH and NADPH oxidase activity in cultured vascular smooth muscle cells. *Circ Res.* 1994;74(6):1141–1148. doi: 10.1161/01.res.74.6.1141.
15. Garrido AM, Griendling KK. NADPH oxidases and angiotensin II receptor signaling. *Mol Cell Endocrinol.* 2009;302(2):148–158. doi: 10.1016/j.mce.2008.11.003.
16. Asehnoune K, Strassheim D, Mitra S, Kim JY, Abraham E. Involvement of reactive oxygen species in Toll-like receptor 4-dependent activation of NF-kappa B. *J Immunol.* 2004;172(4):2522–2529. doi: 10.4049/jimmunol.172.4.2522.
17. Pourheydar B, Samadi M, Habibi P, Nikibakhsh AA, Naderi R. Renoprotective effects of tropisetron through regulation of the TGF-β1, p53 and matrix metalloproteinases in streptozotocin-induced diabetic rats. *Chem Biol Interact.* 2021;335:109332. doi: 10.1016/j.cbi.2020.109332.
18. Takai S, Jin D, Ohzu M, Tanaka K, Miyazaki M. Chymase inhibition provides pancreatic islet protection in hamsters with streptozotocin-induced diabetes. *J Pharmacol Sci.* 2009;110(4):459–465. doi: 10.1254/jphs.09115fp.
19. Jin D, Ueda H, Takai S, et al. Effect of chymase inhibition on the arteriovenous fistula stenosis in dogs. *J Am Soc Nephrol.* 2005;16(4):1024–1034. doi: 10.1681/ASN.2003121009.
20. Terai K, Jin D, Watase K, Imagawa A, Takai S. Mechanism of albuminuria reduction by chymase inhibition in diabetic mice. *Int J Mol Sci.* 2020;21(20):7495. doi: 10.3390/ijms212074.
21. Vibhushan S, Bratti M, Montero-Hernández JE, et al. Mast cell chymase and kidney disease. *Int J Mol Sci.* 2020;22(1):302. doi: 10.3390/ijms22010302.
22. Caughey GH, Raymond WW, Wolters PJ. Angiotensin II generation by mast cell alpha- and beta-chymases. *Biochim Biophys Acta.* 2000;1480(1-2):245–257. doi: 10.1016/s0167-4838(00)00076-5.
23. Andersson MK, Karlson U, Hellman L. The extended cleavage specificity of the rodent beta-chymases rMCP-1 and mMCP-4 reveal major functional similarities to the human mast cell chymase. *Mol Immunol.* 2008;45(3):766–775. doi: 10.1016/j.molimm.2007.06.360.
24. Masuda H, Tanaka T, Takahama. Cisplatin generates superoxide anion by interaction with DNA in

a cell-free system. *Biochem Biophys Res Commun.* 1994;203(2):1175–1180. doi: 10.1006/bbrc.1994.2306.
25. Davis CA, Nick HS, Agarwal AJ. Manganese superoxide dismutase attenuates Cisplatin-induced renal injury: importance of superoxide. *Am Soc Nephrol.* 2001;12 (12):2683–2690. doi: 10.1681/ASN.V12122683.
26. Kelly KJ, Meehan SM, Colvin RB, Williams WW, Bonventre JV. Protection from toxicant-mediated renal injury in the rat with anti-CD54 antibody. *Kidney Int.* 1999;56(3):922–931. doi: 10.1046/j.1523-1755.1999.00629.x.
27. Ramesh G, Reeves WB. TNF-α mediates chemokine and cytokine expression and renal injury in cisplatin nephrotoxicity. *J Clin Invest.* 2002;110(6):835–842. doi: 10.1172/JCI15606.
28. Marques-Carvalho A, Kim HN, Almeida M. The role of reactive oxygen species in bone cell physiology and pathophysiology. *Bone Rep.* 2023;19:101664. doi: 10.1016/j.bonr.2023.101664.
29. Li H, Horke S, Förstermann U. Vascular oxidative stress, nitric oxide and atherosclerosis. *Atherosclerosis.* 2014;237(1):208–219. doi: 10.1016/j.atherosclerosis.2014.09.001.
30. Asami J, Shimizu, T. Structural and functional understanding of the toll-like receptors. *Protein Sci.* 2021;30(4):761–772. doi: 10.1002/pro.4043.
31. Sherif IO, Al-Mutabagani LA, Alnakhli AM, Sobh MA, Mohammed HE. Renoprotective effects of angiotensin receptor blocker and stem cells in acute kidney injury: involvement of inflammatory and apoptotic markers. *Exp Biol Med.* 2015;240(12):1572–1579. doi: 10.1177/1535370215577582.
32. Atwa AM, Abd El-Ghafar OAM, Hassanein EHM, et al. Candesartan attenuates cisplatin-induced lung injury by modulating oxidative stress, inflammation, and TLR-4/NF-κB, JAK1/STAT3, and Nrf2/HO-1 signaling. *Pharmaceuticals.* 2022;15(10):1222. doi: 10.3390/ph15101222.

Received February 26, 2024
Accepted April 10, 2024